Complexity of mixed allotropes of MoS_2 unraveled by first-principles theory

Raquel Esteban-Puyuelo [1,*] D. D. Sarma [2,†] and Biplab Sanyal [1,‡]

[1]*Division of Materials Theory, Department of Physics and Astronomy, Uppsala University, Box-516, SE 75120, Sweden*

[2]*Solid State and Structural Chemistry Unit, Indian Institute of Science, Bengaluru - 560012, India*

(Received 26 June 2020; revised 24 August 2020; accepted 8 October 2020; published 20 October 2020)

Two-dimensional MoS_2 forms stable and several metastable allotropes of semimetallic, metallic, and semiconducting characters, depending on the experimental growth conditions. In this paper we consider intergrowth of the two most frequently reported metastable phases of MoS_2 ($1T$ and $1T'$) within the stable $1H$ phase to establish the effect of geometric and electronic reconstructions of the interface region between $1H$ and $T/1T'$ phases using first-principles density functional calculations. We show that a complex structural reconstruction at the interfaces is responsible for the opening of an energy gap driving the electronic and geometric structures to resemble that of the $1T'$ phase. It is also found that the size of the patches inside the $1H$ matrix crucially controls the geometry and electronic structure close to the Fermi level. These results establish that remarkable properties of chemically exfoliated MoS_2 with patches of metastable structures are to be understood as arising fundamentally from intergrowths necessarily strained due to lattice mismatch across the interface between the H and the distorted T phase, rather than in terms of any pure metastable phase.

DOI: 10.1103/PhysRevB.102.165412

I. INTRODUCTION

The experimental realization of graphene in 2004 [1] boosted the interest on two-dimensional (2D) materials, which can be synthesized by mechanical or chemical exfoliation from van der Waals bonded 2D layers in a bulk phase. Since graphene is a semimetal and thus has a very poor on-off ratio, its range of applicability as an alternative to silicon in semiconductor devices is very limited. One of the options extensively researched in this context is based on 2D transition metal dichalcogenides (TMDs) [2–5].

MoS_2 is the lightest member of the TMD family and it has been studied for decades because it is very abundant in the Earth's crust. It is broadly used as a catalyst [6,7] and solid state lubricant [8,9]. Much like graphite, it is a layered material in which the layers are stacked via van der Waals forces. However, each layer in MoS_2 is in its turn formed by three atomic layers with a thickness of 6.2 Å [10], in which a central molybdenum layer is sandwiched between two sulfur layers. Monolayer MoS_2 is easy to obtain experimentally via mechanical exfoliation. Another route is chemical exfoliation: ion intercalation is possible [11] due to the weak van der Waals forces between the layers, which increases the separation between the layers progressively until the interlayer coupling is insignificant [12]. A recent review article [13] discusses the aspects of chemically exfoliated 2D MoS_2.

Bulk MoS_2 has an indirect gap of 1.2 eV [14] but the monolayer is, in its ground state phase, a direct gap semiconductor (1.8 eV) at the high symmetry point K in the Brillouin zone [4]. This, together with its abundance and convenient mechanical properties, has made it interesting for material scientists, leading to exponential increase in the recent publication [11]. Among other applications, 2D MoS_2 is a promising candidate for transparent and flexible electronics [3,15,16].

Monolayer MoS_2 can exist in different structural phases, three of the most commonly discussed in the literature are shown in Fig. 1. The ground state phase is $1H$, in which the S and Mo atoms are stacked in an A-B-A fashion, so that S atoms are on top of each other and six S atoms are bonded to the central Mo atom in a trigonal coordination. This phase is, as mentioned before, a direct semiconductor of 1.8 eV band gap, and it has been extensively studied theoretically and experimentally [10,11]. Higher energy polymorphs are rather common as patches in the $1H$ phase when extracting monolayer MoS_2 via chemical exfoliation, and have an A-B-C stacking with octahedral coordination of S atoms around the central Mo. The pure $1T$ phase, which can be attained from the $1H$ via a gliding displacement of one of the S atomic planes, is dynamically unstable. This means that it will spontaneously undergo Jahn-Teller distortions towards one of the stable or metastable phases that have been found so far. The lowest energy metastable phase is called $1T'$ phase. It is obtained from $1T$ via the dimerization of the Mo atoms (see Fig. 1), so that there is an alternation of short and long Mo-Mo bonds, which lowers the energy. While the above discussion relates to the pure form of each phase, in practice, the metastable phases invariably appear as small patches intergrown within the stable $1H$ phase. Consequently, in contrast

*Corresponding author: raquel.esteban@physics.uu.se
†sarma@iisc.ac.in
‡biplab.sanyal@physics.uu.se

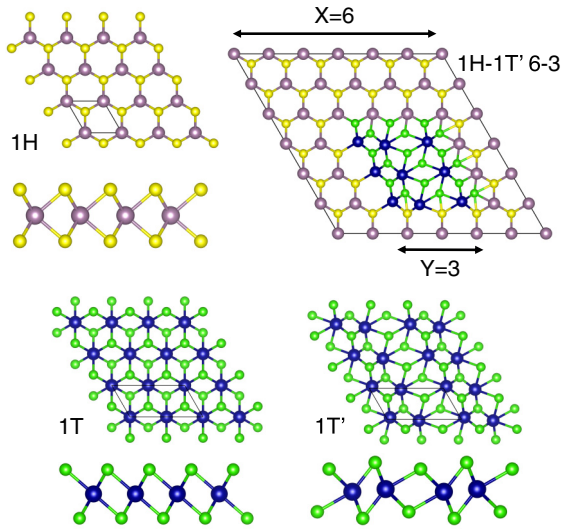

FIG. 1. Three different phases of monolayer MoS_2: the ground state trigonal $1H$ and the two octahedral polytopes, $1T$ and $1T'$. Mo atoms are shown in purple in $1H$ and blue in $1T$ and $1T'$, while S atoms are yellow in $1H$ and green in $1T$ and $1T'$. Different colors have been used to distinguish the mixed phase structures in the rest of the paper. An example of these is included in the right top panel: the $1H$ matrix is a 6×6 supercell, making $X = 6$, and the octahedral patch is 3×3, so that $Y = 3$. Since the patch is in this case $1T'$, this structure is named $1H$-$1T'$ 6-3.

to the considerable research carried out for the $1H$ phase, fewer studies are available on these octahedral forms, and most of them are theoretical works due to the difficulty to spatially resolve the small patches experimentally with photoemission spectroscopy [17].

The $1T$ phase is known to be metallic [18], which could be beneficial for some applications such as supercapacitors [19], if there was a way of stabilizing it. In fact, it has been implicitly hoped for that the instability of the pure $1T$ phase may be alleviated when it is formed as small patches of intergrowth areas within the stable $1H$ phase. The calculated electronic structure of dimerized $1T'$ phase exhibits a small gap in the presence of spin-orbit coupling, though the magnitude of this gap somewhat varies across different calculations [2,20]. In a recent paper [2], the metastable trigonal $1T'$ phase has been observed in experiments within the matrix of hexagonal $1H$ phase yielding a band gap around 90 meV, supported by theoretical calculations of bulk phase using *GW* method. It is extremely challenging to experimentally assess which of the metastable phases is found in experiments, because they usually coexist with the $1H$ phase as small patches, which imply finite size effects, strain, charge doping, etc. This complicates the interpretation of the results and leads to conflicting reported results [13]. Therefore, understanding the structural and electronic properties of these composites is nontrivial. Even theoretically, very little attention has been drawn to the interfaces between these phases while mostly pure phases have been investigated. There are extensive experimental reports on the topic of phase boundaries and phase transitions between the different phases in 2D transition metal dichalcogenides [21–23], and several theoretical works that describe phase transitions [24–26], but to our knowledge, only a recent publication [27] on lateral heterostructures of $1H$ and $1T$ phases of MoS_2 tackles the very important aspect of the phase coexistence from the theoretical point of view. A detailed understanding of the atomic structure and properties of the interfaces between different phases of MoS_2 is of paramount importance because, besides their academic interest, heterostructures combining such phases can potentially be used in efficient nanodevices [24,25,28].

In this study we explicitly investigate the interfaces between $1H$ and two most relevant octahedral phases ($1T$ and $1T'$) to provide an insight into the extensive reconstructions within the patches and at the boundaries and corresponding electronic structures. We have chosen to study the $1T$ form and the first metastable polymorph ($1T'$). The $1T$ phase is unstable from group symmetry arguments, but those analyses assume long-range periodicity. Therefore, the possibility of achieving locally metastable $1T$ phases coexisting as small patches in the $1H$ host is still open. For this purpose, we have constructed mixed phases of monolayer MoS_2 combining the ground state trigonal phase $1H$ acting as a matrix and one of the octahedral polymorphs $1T$ and $1T'$ as a patch. Three different supercell sizes have been considered so that the spatial region of the $1H$ phase between the periodic images of the patches is kept constant while the patch grows. We name the structures $1H$-$1P$ X-Y, $1P$ being the polymorph type ($1T$ or $1T'$) that we start with, X being the size of the $1H$ supercell matrix, and Y being the size of the octahedral phase patch, in units of a hexagonal 1×1 unit cell, as Fig. 1 shows. The models have been constructed in accordance with the results reported in [27], which found that armchair boundaries lead to atomic migration and therefore have been avoided in this study, in favor of the very stable zigzag interfaces. Furthermore, and following the naming convention in the aforementioned study, each patch has Mo interfaces to the top and right and S interfaces to the bottom and left. It is important to note here that the label of $1H$-$1T$ or $1H$-$1T'$ only represents the starting geometry of the internal patch before optimization. The geometry optimization carried out for each of these supercells make extensive changes in the internal structures, such that one may not see any resemblance of the final atomic arrangements to the starting one, as discussed in detail later.

The paper is organized as follows. In the next section we discuss the effects of strain on the band structure of pure 2D phases of $1T$ and $1T'$. Then we present a detailed analysis of the geometries and electronic structures of the mixed phases and discuss several scenarios of gap opening. Thereafter, we summarize our findings and discuss their implications. Finally, we provide the details of the computational methods. We provide Supplemental Material (SM) as an external file where we include additional figures [29].

II. METHODOLOGY

All calculations were done in the framework of density functional theory (DFT) using the projector augmented wave (PAW) [30,31] method and the Perdew-Burke-Ernzerhof (PBE) generalized-gradient approximation (GGA) [32] implemented in the Vienna *ab initio* simulation package (VASP)

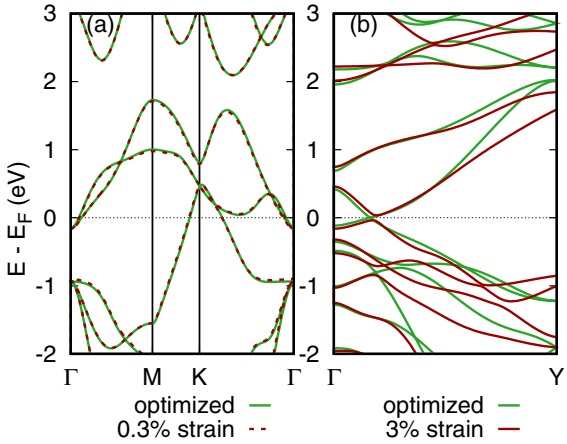

FIG. 2. Effect of strain on the band structure of the octahedral phases. Band structure of $1T$ (a) and $1T'$ (b) MoS_2. The green solid line represents the band structure of the cell that minimized the total energy with respect to the variation of the lattice parameter in each of the phases. The dashed (solid) red line depicts the band structure of the $1T$ ($1T'$) under the strain that the 1H equilibrium lattice parameter imposes.

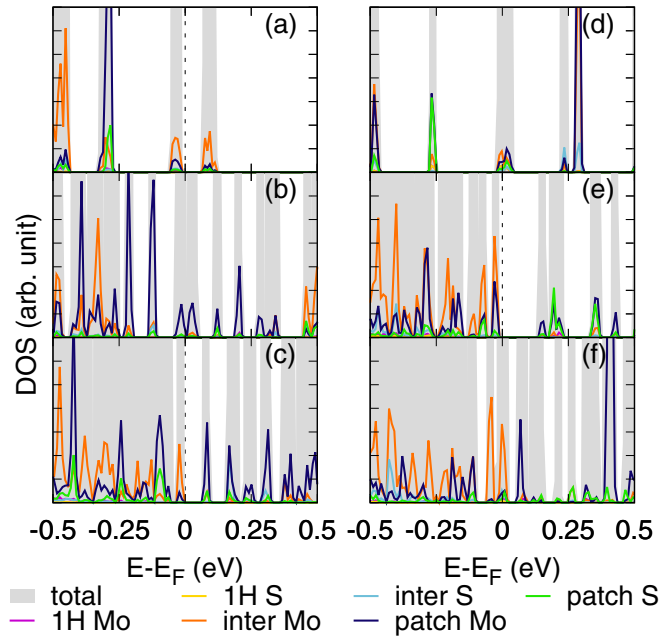

FIG. 3. Contribution to each kind of atomic type to the DOS of the six structures close to the Fermi energy. (a), (b), and (c) Represent the $1H$-$1T$ 6-3, 9-6, and 12-9 composites, respectively. (d), (e), and (f) Represent the $1H$-$1T'$ 6-3, 9-6, and 12-9 composites, respectively. The gray filled curves are the peaks from the total DOS of each structure, and the solid lines are the partial DOS of selected Mo and S atoms belonging to bulk $1H$ (purple and yellow, respectively), the interfacial region (orange and light blue, respectively), and the bulk region of the patch, either $1T$ for the left panel or $1T'$ for the right one (dark blue and green). Gap opening happens for (a), (c), and (e).

[33–35] code, which uses a plane-wave basis. We have used a cutoff of 400 eV to truncate the plane-wave basis representing the Kohn-Sham orbitals. For the geometry optimization, the Brillouin zone was sampled by the Γ point and the atomic positions were relaxed until the force per atom is less than 0.005 eV/Å using the conjugated gradient method. A denser $3 \times 3 \times 1$ Monkhorst-Pack mesh was used for the self-consistent description of the electronic states and density of states (DOS).

III. RESULTS AND DISCUSSION

A. Strain dependence of pure phases

The three considered phases of MoS_2 have different lattice parameters. However, we have constructed the mixed phases supercells using the lattice parameter (3.190 Å) of the $1H$ phase since it is the most stable and common phase and acts as the host matrix. The lattice parameters that minimize the total energy in pure 2D $1T$ and $1T'$ phases are 3.200 Å for $1T$ and 3.275 and 6.600 Å for $1T'$. This means that the octahedral patches will be subjected to planar compressive strain, and this structural change may affect their electronic properties. The $1T$ phase is strained only 0.3% and it is a very stable metallic phase, so its band structure does not undergo any relevant changes, as shown in Fig. 2. However, in its optimized lattice parameter, the $1T'$ phase is a semimetal with bands crossing only at one reciprocal lattice point in the Brillouin zone. The nearly 3% compressive strain it is subjected to when placed in the $1H$ matrix is able to open up a small gap, as Fig. 2 shows, in line with what was reported previously [36].

B. Mixed phases

1. Electronic structure

The atomic positions within the mixed phase supercells, described in the Introduction, were optimized to minimize the energy in each case. Therefore, the final structures are not composed of perfect $1H$, $1T$, or $1T'$ phases due to the reorganization of the atomic positions. First we study the density of states (DOS) of the resulting supercells, focusing on the range of energies close to the Fermi energy, shown in Fig. 3. The two kinds of starting supercells seem to behave in an opposite way after structural relaxation, while there is a clear trend towards a gap opening after relaxation: $1H$-$1T$ 6-3 and $1H$-$1T$ 12-9 show a gap opening of 84 and 85 meV, respectively, while $1H$-$1T$ 9-6 does not. On the contrary, $1H$-$1T'$ 6-3 and $1H$-$1T'$ 12-9 are metallic but $1H$-$1T'$ 9-6 has a gap of 167 meV. To explain this, we compare the total energies of these structures, reported in Table I: the gapped systems have lower energy than their metallic counterparts for every size considered. This means that whichever phase the patch started in ($1T$ or $1T'$), the systems, independent of the patch size, evolve towards a

TABLE I. Total energies (in eV) and values of the gap of the mixed phases. Bold indicates the lowest energy structure of each size, which opens up a gap, included in parentheses (in meV).

	$1H$-$1T$	$1H$-$1T'$
6-3	**−770.40** (84)	−770.01
9-6	−1729.82	**−1730.08** (167)
12-9	**−3070.11** (85)	−3068.48

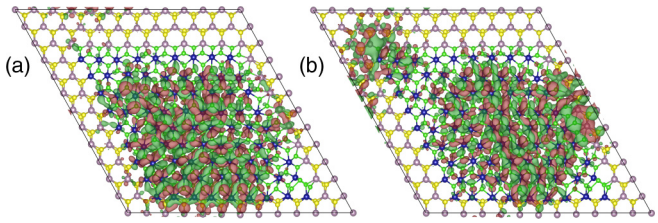

FIG. 4. Charge density of the VBM (a) and CBM (b) in $1H$-$1T$ 12-9. The red (green) color represents positive (negative) charge density with an isovalue $4.88 \times 10^{-6} e/\text{Å}^3$.

gapped electronic structure because it is energetically favorable. This suggests that stabilizing an intrinsically metallic patch of a metastable phase of MoS_2 as an intergrowth inside a $1H$ matrix, independent of the patch size, is an improbable event due to energy considerations. Even when the starting atomic arrangements of the patch mimics that of the $1T$ metallic phase, we find that the lowest energy configuration invariably takes on a small gapped semiconducting nature following atomic rearrangements to accommodate the resulting strain across the interface. A plausible explanation to why the starting $1H$-$1T'$ did not result in a ground state for 6-3 and 12-9 can be related to even-odd effects. These configurations have an odd number of Mo atoms in the patch, which means that one interface Mo atom is left to dimerize with another Mo originally belonging to the $1H$ host. This is, for an odd size of the patch, less favorable than the starting $1H$-$1T$ arrangement in which the Mo-Mo bonds are more similar. Additionally, the emergence of a gap, even for the starting T phase patch, cannot be attributed to strain, as it has been shown in Fig. 2 that the T phase is impervious to strain and remains metallic.

We have plotted the partial densities of states of selected atoms belonging to different regions in the composite, i.e., Mo and S atoms in the $1H$ bulk, in the $1T$ or $1T'$ bulk region, and in the interfacial region between the two phases. As shown in Fig. 3, the states contributing mostly to the DOS close to the gap belong to Mo atoms in the bulk of the octahedral patch or Mo atoms in the interfacial region between the patch and the $1H$ host. The host states, both belonging to Mo and S, are further away from the composite gap, as the pure $1H$ phase has a gap of 1.8 eV, much larger than the small gap (tens of meVs) openings due to geometrical reconstructions. This is represented in Fig. 1 in the SM [29] for the $1H$-$1T$ and $1H$-$1T'$ 12-9 structures, in which the Mo and S states of the $1H$ phase are represented in purple and yellow, respectively, and are far from the gap. It is clearly seen that the electronic states emerging in the band gap of the $1H$ host originate from the $1T$ or $1T'$ patches. Moreover, these states are not localized on particular atoms, but they are extended over the whole patch and interfacial regions. As an example, we provide the charge density isosurfaces of the valence band maximum (VBM) and conduction band minimum (CBM) in $1H$-$1T$ 12-9 in Fig. 4.

In order to further study the effect of the reconstruction, we turn to Fig. 2 in the SM [29], which shows the total DOS of each structure before and after structural relaxation. As apparent by the changes of the peaks, the gaps open only in the relaxed structures, since all the structures were metallic before allowing the atoms to relax to their lowest energy positions. Therefore, the gap opening can be attributed to the atomic relaxation, which in turn affects the electronic structure.

2. *Structural reconstruction*

Interestingly, the extent of the structural distortion is not limited to the boundary between the phases. Figures 5 and 6 illustrate this for the lowest energy structures, which show gap opening, and Fig. 3 in the SM [29] includes the high energy ones, which are metallic.

The comparison between the atomic positions before (in the gray background) and after relaxation show a clear displacement of the atoms, which is in general larger for the supercells that have a starting $1T$ patch, compared to $1T'$. The smallest cell (6-3) patches show larger distortions than the larger ones, since the interface has a very strong effect. Reconstruction is very clear for corner atoms, specially S, as highlighted in Figs. 5(e) and 5(f) for $1H$-$1T$, but also present in $1H$-$1T'$. The S atoms in the $1H$ phase shift laterally in the $1H$-$1T$ composites [Fig. 5(g)], but this is less evident in $1H$-$1T'$ (Fig. 6), which overall suffers less changes. Nonetheless, structural distortions reach the center of the 12-9 patches, as evident in Figs. 5(h) and 6(c), in which a clear tendency towards Mo-Mo dimerization after relaxation is revealed. This is responsible for the larger degree of position changes in the $1H$-$1T$ structures compared to the $1H$-$1T'$. The combination of short and long bonds, which is a characteristic of the $1T'$ phase, is also accompanied by a vertical shift in the S positions, so that the S atoms in a long Mo-Mo bond come closer to the center of the layer and the ones in a short Mo-Mo bond go further away [see Figs. 5(d) and 6(d)]. This disposition towards a $1T'$-like phase in the patches of the mixed supercells can be explained by the relative stability of their pure phases, since $1T'$ has a much lower energy than the unstable $1T$. It should be noted that, even if the general trend of the patches is to reconstruct towards a $1T'$-like phase, there can be regions in which the atomic positions may locally retain a $1T$ type arrangement, specially in the $1H$-$1T$ interfaces like exemplified by Fig. 6(c). This could be an explanation to why the $1T$ phase seems to have been observed in transmission electron microscopy experiments, even if it is high in energy compared to $1T'$ and the ground state $1H$ phases.

To clearly asses how the structural reconstruction induces Mo-Mo dimerization in the mixed phases both in the boundary and center of the patches, we have plotted histograms for the nearest neighbors (NNs) of Mo (either Mo or S atoms) in Fig. 7. A histogram for the pure phases would only have counts at the characteristic NN distances that are marked with vertical lines and the spread around those distances is the mere effect of the interface distortions, which cannot be captured by theoretically studying pure phases only. In all the histograms, the first dome (2.3–2.6 Å distances) belongs to Mo-S bonds and the second one (3–3.4 Å) corresponds to Mo-Mo distances.

As expected, most of the NN distance counts in the $1H$-$1T$ supercells are concentrated around the corresponding distances for pure $1H$ and $1T$ phases. In the same way, the NN distances in $1H$-$1T'$ are centered around those of the pure $1H$ and $1T'$ phases. However, the distributions in the top row

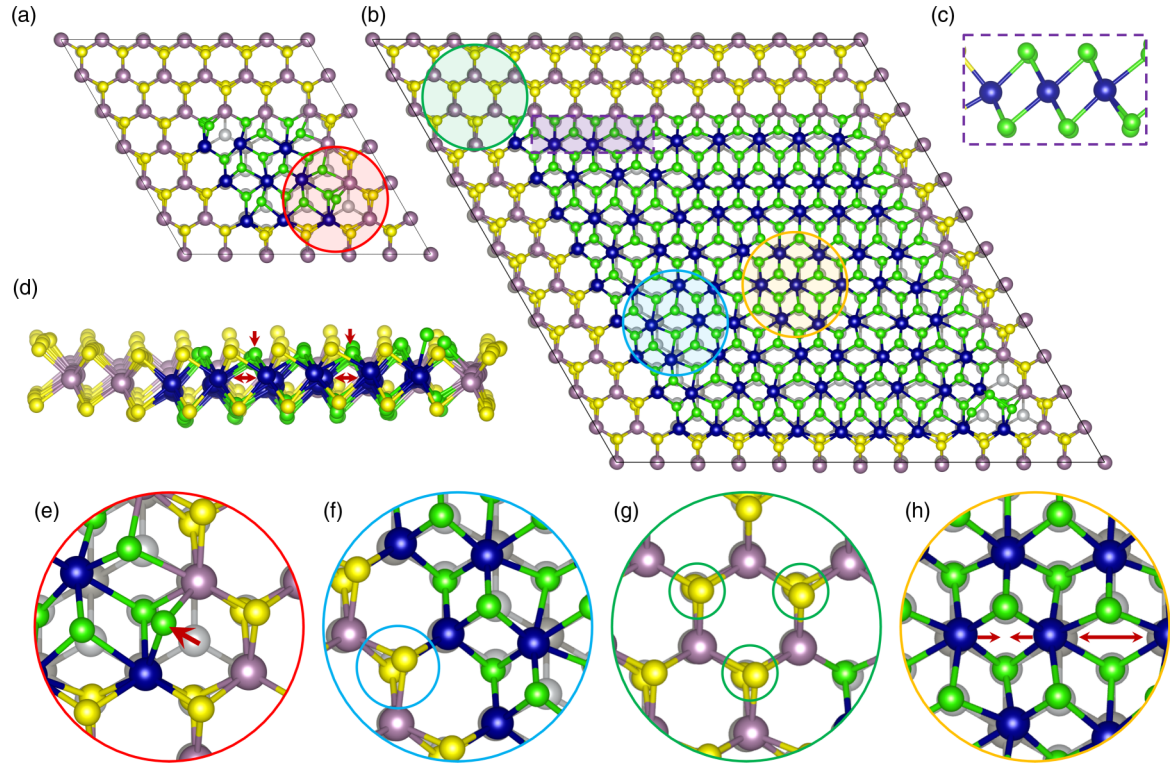

FIG. 5. Structural reconstruction in the $1H$-$1T$ low energy composites [6-3 in (a) and 12-9 in (b)]. Overlapping atomic positions before (gray) and after relaxation (following the color coding described in Fig. 1). (c) Side view of the dashed purple rectangle in (b). (d) Side view of the $1H$-$1T$ 9-6 in which the arrows point at the Mo-Mo dimerization features. (e)–(h) Zoomed regions enclosed by colored circles in (a) and (b). The arrow in (e) highlights a large atomic displacement, and the arrows in (h) show the direction of the Mo relaxation towards its dimerized positions.

(starting $1T$ patch) and the lower row (starting $1T'$ patch) are not very different for each size: $1H$-$1T$ structures show also the presence of $1T'$ characteristic distances, specially the 2.73 Å of the Mo-Mo short bond, in all its sizes (6-3, 9-6, and 12-9). This confirms that the reconstruction goes towards a common mixed structure with traces of Mo-Mo dimerization just as the $1T'$ phase has, which is what we had visually assessed before. Furthermore, it is interesting to see that even if the supercells have been designed as multiples of the $1H$ unit cell with the corresponding lattice parameter, the atoms in the patches are able to rearrange themselves into the $1T'$ bond lengths. Therefore, given that the pure strained $1T'$ phase is a small gap semiconductor, the tendency of the mixed structures to open a gap after relaxation can be rationalized. As a note, the fact that the dimerization is more apparent in the larger cells can be explained by the better statistics provided by a larger number of bonds.

IV. CONCLUSION

We have presented a detailed study of the interface reconstruction of heterostructures of different structural phases

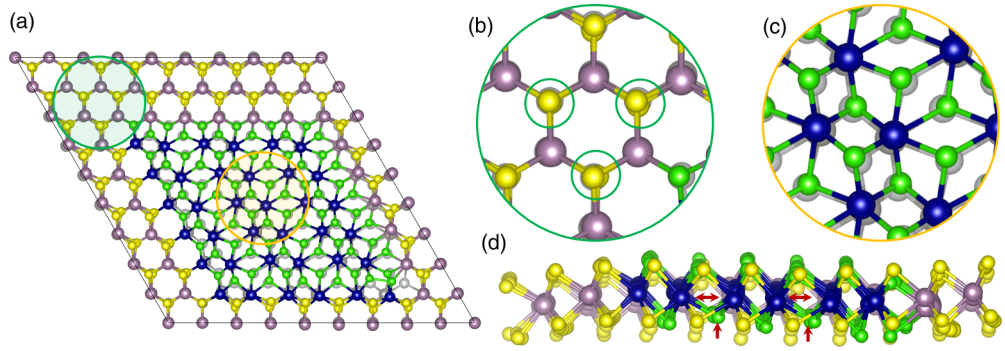

FIG. 6. Structural reconstruction in the $1H$-$1T'$ 6-3 composite. (a) Overlapping atomic positions before (gray) and after relaxation (following the color coding described in Fig. 1). (b) and (c) Zoomed regions enclosed by colored circles in (a). (d) Lateral view of (a) with arrows highlighting the features of Mo-Mo dimerization.

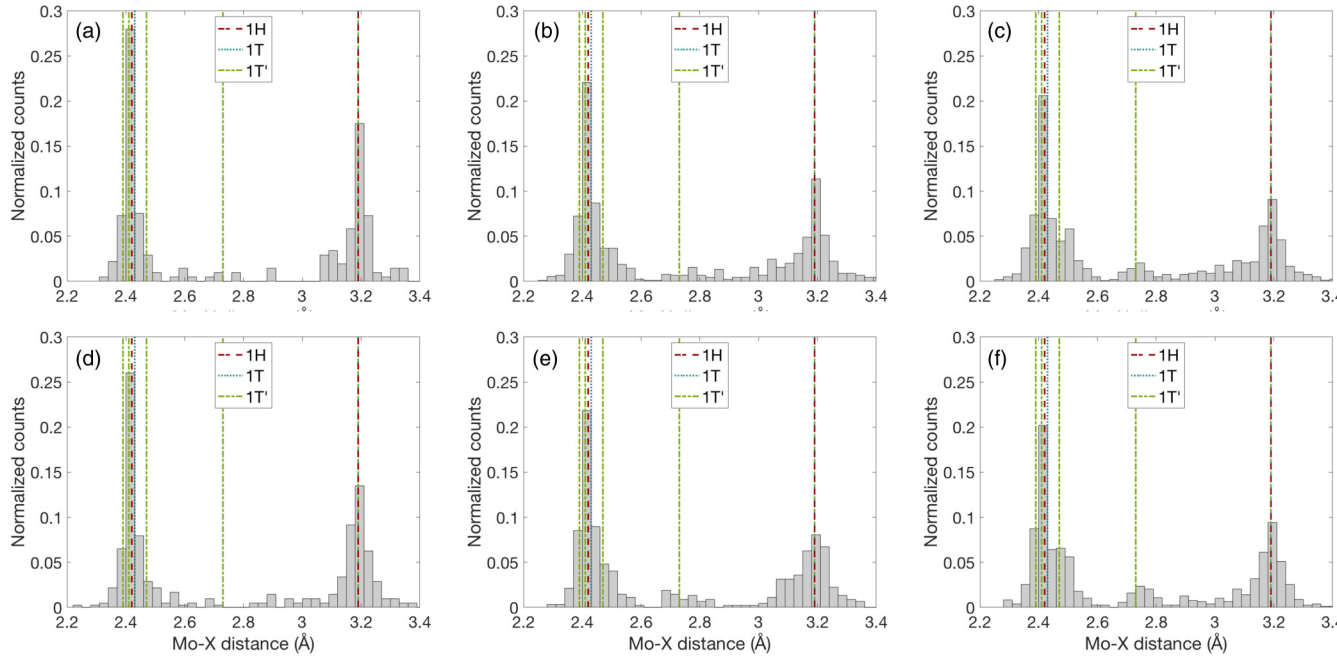

FIG. 7. Probability normalized histograms of the Mo-X distance, X being a Mo nearest neighbor atom (Mo or S). (a)–(c) 6-3, 9-6, and 12-9 $1H$-$1T$, respectively. (d)–(f) 6-3, 9-6, and 12-9 $1H$-$1T'$, respectively. The vertical lines denote the pure phases nearest neighbor distances (red dashed for $1H$, blue dotted for $1T$, and green dash-dotted line for $1T'$).

of monolayer MoS_2 by density functional theory. Our study reveals that this reconstruction is essential to explain the electronic structure of the composites, as they cannot be described simply by the behavior of pure phases. The interaction between the trigonal ground state phase ($1H$) and any of the octahedral phases ($1T$ and $1T'$) results in a reorganization of the atoms in the metastable octahedral patch that generates a dimerization of the Mo atoms similar to what happens in the $1T'$ structure. This structural change is responsible for the opening of a small gap in the density of states of the composite structure, leading to a semiconducting nature. The importance of the structural reconstruction and gap opening in the samples having coexisting phases of MoS_2 clarifies a key aspect needed for explaining the broad variety of experimental reports on the subject.

ACKNOWLEDGMENTS

B.S. acknowledges financial support from the project grant (2016-05366) and Swedish Research Links programme grant (2017-05447) from Swedish Research Council. D.D.S. thanks the Science and Engineering Research Board, Department of Science and Technology, Government of India, and Jamsetji Tata Trust for supporting this research. R.E. thanks X. Chen for fruitful discussions and F. Schrodi for assistance with the histogram calculations. R.E. acknowledges the Swedish National Infrastructure for Computing (SNIC) for the allocation of computing time in Tetralith, NSC. Moreover, supercomputing resources from PRACE DECI-15 project DYNAMAT are gratefully acknowledged.

[1] A. K. S. Novoselov, A. K. Geim, S. V. Morozov, D. A. Jiang, Y. Zhang, S. V. Dubonos, I. V. Grigorieva, and A. A. Firsov, Science **306**, 666 (2004).
[2] B. Pal, A. Singh, G. Sharada, P. Mahale, A. Kumar, S. Thirupathaiah, H. Sezen, M. Amati, L. Gregoratti, U. V. Waghmare, and D. D. Sarma, Phys. Rev. B **96**, 195426 (2017).
[3] A. Splendiani, L. Sun, Y. Zhang, T. Li, J. Kim, C. Y. Chim, G. Galli, and F. Wang, Nano Lett. **10**, 1271 (2010).
[4] K. F. Mak, C. Lee, J. Hone, J. Shan, and T. F. Heinz, Phys. Rev. Lett. **105**, 136805 (2010).
[5] Y. Sun, S. C. Wu, M. N. Ali, C. Felser, and B. Yan, Phys. Rev. B **92**, 161107(R) (2015).
[6] E. Devers, P. Afanasiev, B. Jouguet, and M. Vrinat, Catal. Lett. **82**, 13 (2002).
[7] W. Zhong, W. Tu, S. Feng, and A. Xu, J. Alloys Compd. **772**, 669 (2019).
[8] G. Salomon, A. W. De Gee, and J. H. Zaat, Wear **7**, 87 (1964).
[9] M. Chhowalla and G. A. Amaratunga, Nature (London) **407**, 164 (2000).
[10] R. G. Dickinson and L. Pauling, J. Am. Chem. Soc. **45**, 1466 (1923).
[11] I. Song, C. Park, and H. C. Choi, RSC Adv. **5**, 7495 (2015).
[12] G. Eda, H. Yamaguchi, D. Voiry, T. Fujita, M. Chen, and M. Chhowalla, Nano Lett. **11**, 5111 (2011).
[13] D. Pariari and D. D. Sarma, APL Mater. **8**, 040909 (2020).
[14] T. Böker, R. Severin, A. Müller, C. Janowitz, R. Manzke, D. Voß, P. Krüger, A. Mazur, and J. Pollmann, Phys. Rev. B **64**, 235305 (2001).

[15] B. Radisavljevic, A. Radenovic, J. Brivio, V. Giacometti, and A. Kis, Nat. Nanotechnol. **6**, 147 (2011).
[16] Q. H. Wang, K. Kalantar-Zadeh, A. Kis, J. N. Coleman, and M. S. Strano, Nat. Nanotechnol. **7**, 699 (2012).
[17] D. Pariari, R. M. Varma, M. N. Nair, P. Zeller, M. Amati, L. Gregoratti, K. K. Nanda, and D. D. Sarma, Appl. Mater. Today **19**, 100544 (2020).
[18] F. Wypych and R. Schöllhorn, J. Chem. Soc. Chem. Commun. **19**, 1386 (1992).
[19] M. Acerce, D. Voiry, and M. Chhowalla, Nat. Nanotechnol. **10**, 313 (2015).
[20] M. Calandra, Phys. Rev. B **88**, 245428 (2013).
[21] G. Eda, T. Fujita, H. Yamaguchi, D. Voiry, M. Chen, and M. Chhowalla, ACS Nano **6**, 7311 (2012).
[22] Y. C. Lin, D. O. Dumcenco, Y. S. Huang, and K. Suenaga, Nat. Nanotechnol. **9**, 391 (2014).
[23] M. M. Ugeda, A. Pulkin, S. Tang, H. Ryu, Q. Wu, Y. Zhang, D. Wong, Z. Pedramrazi, A. Martín-Recio, Y. Chen, F. Wang, Z. X. Shen, S. K. Mo, O. V. Yazyev, and M. F. Crommie, Nat. Commun. **9**, 3401 (2018).
[24] K.-A. N. Duerloo, Y. Li, and E. J. Reed, Nat. Commun. **5**, 4214 (2014).
[25] W. Zhao and F. Ding, Nanoscale **9**, 2301 (2017).
[26] Q. Jin, N. Liu, B. Chen, and D. Mei, J. Phys. Chem. C **122**, 28215 (2018).
[27] X. Zou, Z. Zhang, X. Chen, and B. I. Yakobson, J. Phys. Chem. Lett. **11**, 1644 (2020).
[28] R. Kappera, D. Voiry, S. E. Yalcin, B. Branch, G. Gupta, A. D. Mohite, and M. Chhowalla, Nat. Mater. **13**, 1128 (2014).
[29] See Supplemental Material at http://link.aps.org/supplemental/10.1103/PhysRevB.102.165412 for details on DOS and atomic positions before and after relaxation.
[30] P. E. Blöchl, Phys. Rev. B **50**, 17953 (1994).
[31] G. Kresse and D. Joubert, Phys. Rev. B **59**, 1758 (1999).
[32] J. P. Perdew, K. Burke, and M. Ernzerhof, Phys. Rev. Lett. **77**, 3865 (1996).
[33] G. Kresse and J. Hafner, Phys. Rev. B **47**, 558 (1993).
[34] G. Kresse and J. Furthmüller, Phys. Rev. B **54**, 11169 (1996).
[35] G. Kresse and J. Furthmüller, Comput. Mater. Sci. **6**, 15 (1996).
[36] T. Hu, R. Li, and J. Dong, J. Chem. Phys. **139**, 174702 (2013).